Transparent hydrophobic durable low moisture permeation poly(fluoroimide acrylate)/SiO_2 nanocomposite from solventless photocurable resin system†

Chien-Chih Lin,[a] Sheng-Hao Hsu,[a] Yuan-Ling Chang[b] and Wei-Fang Su*[ab]

Received 25th November 2009, Accepted 29th January 2010
First published as an Advance Article on the web 1st March 2010
DOI: 10.1039/b924726b

In this article, we report a novel high performance nanocomposite made from environmentally friendly and energy conserving solventless photocurable patternable resin system. The system contains a fluoroimide acrylate oligomer, acrylate monomer, photoinitiator and SiO_2 nanoparticles. The fluoroimide acrylate oligomer was synthesized by reacting 2 mole equivalent of 4,4′-(hexafluoroisopropylidene) diphthalic anhydride (6FDA) with 4,4′-(hexafluoroisopropylidene) diamine (6FpDA) first to form fluoroimide dianhydride, and then further reacting with 2 moles of 2-hydroxy ethyl methacrylate (HEMA). The fluoroimide acrylate oligomer was specially designed with carboxylic acid functionality. As compared with bis-phenol A acrylate oligomer, the fluoroimide acrylate oligomer nanocomposite shows an improvement in both physical properties and chemical properties. This new nanocomposite exhibits good cross hatch adhesive strength (>95% on glass) and unusually high hydrophobicity (>140° contact angle). The nanocomposite also shows excellent transparency (>90% transmission at 400–800 nm for 100 μm film), high thermal stability and mechanical durability. The water absorption and the water vapor permeation of this nanocomposite are reduced to at least one quarter of those of the bis-phenol A acrylate nanocomposite. The chemical characteristics of the fluoroimide acrylate and the formation of nanodomains in the nanocomposite play major roles in providing the outstanding performance.

Introduction

While polymers are light weight, conformable, flexible, and easy to process, they remain relatively poor in thermal, mechanical, optical and electronic performance. On the other hand, inorganic materials usually exhibit good physical properties but they are heavy, rigid and difficult to process. By nanosizing an inorganic material and dispersing it into a polymer to make a nanocomposite,[1–3] it is possible to utilize the merits of both materials. Thus, nanocomposites can be used in wide applications such as high refractive index thin films,[4] optics,[5] waveguides,[6] light emitting diodes,[7] solar cells,[8,9] biomimetic materials[10–12] and so on.

Polyimide related materials have been extensively used in aerospace and electronics because of their good mechanical property and thermal stability.[13,14] On the other hand, fluorinated polymers have the characteristics of low cohesive energy, low surface free energy and low water uptake due to their low polarity. The high electronegativity of the F atom contributes to the strong chemical bond between carbon and fluorine atoms, giving fluorocarbon materials high thermal stability. Photopolymerization of a solventless acrylate system is an advanced process for resin curing due to the short curing time, environmentally-friendly characteristics and low temperature/energy demands. In the electronic industry, UV-curable resins are widely used as sealants or encapsulants for high throughput and heat sensitive devices.[13,14]

Highly transparent, porous and hydrophobic inorganic surfaces have been developed through controlling material morphology using sol-gel processing and calcination.[15–23] However, the high calcination temperature and high porosity limits the materials use in the encapsulation of temperature sensitive devices. Steele *et al.* reported the formation of superoleophobic coatings by spray atomization of ZnO nanoparticle-perfluoro polyacrylate in acetone/water cosolvent. The coating also exhibits high porosity.[24] Sangermano *et al.* have synthesized a fluorinated hydroxy acrylate monomer as a coupling agent and a modifier to fabricate UV-cured hydrophobic organic/inorganic hybrid films with contact angles of 90°.[25] The polymer/SiO_2 nanocomposites have been studied extensively and reviewed recently.[26] However, highly transparent, hydrophobic, durable, low moisture permeation nanocomposites made from a solventless photocurable resin system have never been reported before. In this study, a fluoroimide acrylate oligomer with carboxylic acid functionality has been designed and synthesized that can be blended homogeneously with acrylate monomers, acrylate modified silica nanoparticles and photoinitiator into a resin system. The resin system can be cured with UV irradiation to form a high performance nanocomposite. A 5 micron channel waveguide has been fabricated with the loss of 1.18 db cm^{-1} at 1310 nm (supplementary information). As compared with the poly(bis-phenol A acrylate)/SiO_2 nanocomposite system, the poly(fluoroimide acrylate)/SiO_2 nanocomposite exhibits improvement in both physical properties and chemical properties. It exhibits excellent transparency, unusually high

[a]*National Taiwan University, Institute of Polymer Science and Engineering, Taipei, Taiwan*
[b]*National Taiwan University, Department of Materials Science and Engineering, Taipei, Taiwan*
† Electronic supplementary information (ESI) available: Fig. 1S–5S and Table S1. See DOI: 10.1039/b924726b

hydrophobicity, high adhesive strength, high thermal stability, high mechanical strength, low water absorption and low water vapor permeation.

Experimental

Materials

The following chemicals were purchased and used without further purification. 20–25 nm SiO_2 colloidal solution (MA-ST-M, 40 wt% solid content, Nissan Chemical Industries, Ltd.), 3-(trimethoxysilyl) propyl methacrylate (MPS, 98%, Acros Organics), ethoxylated bisphenol A diacrylate (EOBDA, Sartomer Co., Inc.), neopentyl glycol diacrylate (NPGDA, Sartomer Co., Inc.), 4,4′-(hexafluoroisopropylidene) diphthalic anhydride (6FDA, 99%, Sigma-Aldrich Co.), 4,4′-(hexafluoroisopropylidene) dianiline (6FpDA, 98%, Acros Organics), N,N-dimethylacetamide anhydrous (DMAc, 99.8%, Sigma-Aldrich Co.), acetic anhydride (Acros Organics), hydroquinone (99%, Acros Organics), 2,2-dimethoxy-2-phenyl acetophenone (Irgacure 651, Ciba Inc.), 4-octylphenyl phenyliodonium hexafluoroantimonate (OPIA, UV-9380C, General Electric Co.), tetrahydrofuran (THF, 99.5%, Acros Organics) and methanol (99.98%, Tedia Co., Inc.). Pyridine (99+%, Acros Organics) and 2-hydroxyethyl methacrylate (HEMA, stabilized 98%, Acros Organics), were dehydrated by 3 Å molecular sieve.

Preparation of 3-(trimethoxysilyl) propyl methacrylate (MPS) modified colloidal silica

12.5 g of an MA-ST-M SiO_2 colloidal solution was mixed with 20 g methanol for 10 min. 2.5 g MPS was added into the mixture and reacted at 50 °C for 24 h to obtain MPS modified silica nanoparticle solution.

Synthesis and characterization of photosensitive fluoroimide acrylate (PSFIA)

The precursor of PSFIA, fluoroimide dianhydride (FIDA) was first synthesized from dianhydride and diamine at room temperature in N_2. An excess amount of 6FDA was used to create an imide oligomer with dianhydride end functional groups. 4.09 g 6FDA and 1.5 g 6FpDA (molar ratio of 6FDA and 6FpDA = 2.05 : 1.00) were dissolved in 23 and 11 ml of DMAc respectively, and then diamine solution was added to the dianhydride solution to form amic acid. After stirring the amic acid for 24 h under nitrogen purge, 1.84 g acetic anhydride and 1.79 g pyridine were added to the system. The solution was heated to 90 °C under stirring for 7 h to form FIDA. The reaction mixture was cooled and poured into 50 ml de-ionized water to obtain a white precipitate. After centrifuging at 1000 rpm for 5 min, the product was collected by filtration and dried under vacuum (~1 torr) at 150 °C for 24 h. 4 g FIDA powder was re-dissolved in 24 ml DMAc to form a clear solution then reacted with 0.88 g HEMA and 0.029 g hydroquinone at 75 °C for 24 h in air (the molar ratio of the three compounds is 1 : 2 : 0.073). The reaction mixture was cooled and poured into de-ionized water to obtain white PSFIA powder. After centrifuging separation, the product was dried in a vacuum oven (~1 torr) at 50 °C for 24 h. The yield is about 68%.

The chemical structures of the FIDA and PSFIA were determined by Fourier-transformed infrared (FT-IR) spectroscopy and proton nuclear magnetic resonance (^{1}H NMR) spectroscopy. FT-IR spectra were recorded using a Nicolet Manga-IR500 spectrometer. Specimens were prepared by mixing 1 mg of the sample with 100 mg dried KBr and pressing the mixture into pellets. The spectra were acquired between 400 and 4000 cm^{-1} at a resolution of 4 cm^{-1} and averaged over 32 scans at room temperature. ^{1}H NMR measurement was performed on a Bruker-400 spectrometer. Specimens were prepared by dissolving 30 mg of the sample in 1 ml D-chloroform.

Preparation of solventless photocurable resin system

The compositions of the resin systems, labeled as NES and NPS series, are listed in Table 1. The resin system was prepared according to our established method.[12] The general procedure involves mixing the surface modified SiO_2 nanoparticle solution with a mixture of NPGDA and EOBDA and photoinitiator (Ciba Irgacure 651) or with a mixture of PSFIA and NPGDA and photoinitiator in an Al-foil covered flask that is shielded from light. The mixing is under stirring for one hour at room temperature. Then, the solvent in the mixture was removed using vacuum (~10^{-3} torr) for about one hour to prepare a solventless resin system.

Preparation of nanocomposite samples

The about 100 μm nanocomposite film sample was prepared by casting the solventless photocurable resin system in a polyethylene terephthalate (PET) mould, then cured by UV light (365 nm, 1.86 mW cm^{-2}, ENF-240C, Spectroline) for 2 min in a N_2 chamber. The thickness of the cured nanocomposite film was determined by a thickness gauge (543–690 ID-S112, Mitutoyo Co.). A disk sample of 5 mm (diameter) × 2 mm (thick) was prepared by casting the solventless photocurable resin system in a Teflon model, then cured by a UV light (365 nm, 1.86 mW cm^{-2}) for 5 min on both sides. All UV cured samples are post cured at 100 °C for 12 h. All the samples are examined by differential scanning calorimetry (DSC 2920, TA instrument) to show they are fully cured before subjecting them to different characterizations (see supplementary information).

Preparation of thermally cured PSFIA (T-PSFIA)

In order to study the hydrophobicity of neat PSFIA without reactive monomer NPGDA, a thermal curing process was adopted to fabricate PSFIA film, and this thermal cured PSFIA was named T-PSFIA. The melting point of PSFIA powder is about 140 °C determined by DSC. At 140 °C, most peroxide thermoinitiators and photoinitiators are not stable during the melting of PSFIA. Therefore, a cationic photoinitiator OPIA (thermal decomposition temperature is 166 °C determined by DSC) was used as a thermal initiator to prepare the T-PSFIA film. 1 g PSFIA, 0.04 g OPIA and 25 g THF were homogeneously mixed in an Al-foil covered flask. After stirring for 10 min, THF was removed by rotary evaporator, and the uncured T-PSFIA powder was dried under vacuum (~1 torr) at 50 °C for 24 h. The T-PSFIA film sample was prepared by placing T-PSFIA powder on a glass plate, and melting at 150 °C under N_2 for 10 min. After

Table 1 Compositions and acrylate functionality of T-PSFIA, NES series and NPS series of resin system

Sample	Composition (wt%)[a]					AFN[b]/mol g^{-1}	AFO[c]/mol g^{-1}
	SiO_2	MPS	EOBDA	NPGDA	PSFIA		
NES00	0	0	30.00	70.00	0	7.88E-03	7.88E-03
NES10	9.05	4.52	25.93	60.50	0	6.99E-03	8.45E-03
NES20	18.10	9.05	21.86	51.00	0	6.10E-03	9.10E-03
NES30	27.15	13.57	17.78	41.50	0	5.22E-03	9.83E-03
NES40	36.20	18.10	13.71	31.99	0	4.33E-03	1.06E-02
NES50	45.15	22.62	9.64	22.49	0	3.45E-03	1.15E-02
NES60	54.30	27.15	5.57	12.99	0	2.55E-03	1.22E-02
NPS00	0	0	0	70.00	30.00	6.86E-03	6.86E-03
NPS10	9.05	4.52	0	60.50	25.93	6.11E-03	7.38E-03
NPS20	18.10	9.05	0	51.00	21.86	5.36E-03	7.99E-03
NPS30	27.15	13.57	0	41.50	17.78	4.61E-03	8.69E-03
NPS40	36.20	18.10	0	31.99	13.71	3.86E-03	9.49E-03
NPS50	45.15	22.62	0	22.49	9.64	3.12E-03	1.04E-02
NPS60	54.30	27.15	0	12.99	5.57	2.37E-03	1.13E-02
EOBDA	0	0	100.00	0	0	4.27E-03	4.27E-03
NPGDA	0	0	0	100.00	0	9.42E-03	9.42E-03
T-PSFIA	0	0	0	0	100.00	8.64E-04	8.64E-04

[a] 4 wt% of photoinitiator is used based on the organic component. [b] Acrylate functionality of nanocomposite. [c] Acrylate functionality of organic component of nanocomposite.

the powder melted, the temperature was increased to 170 °C in 10 min and held for 2 h to obtain the T-PSFIA film.

Characterization of the nanocomposite

The TEM nanocomposite ultra thin film samples were prepared at room temperature by ultra-microtomy (Leika EM UC6 ultra-microtome machine and Drukker ultra-microtome knife). A cutting edge of 45° was used to obtain about 80 nm film sample that was then placed on a 200-mesh copper grid. The sample was studied by using a Joel JEM 1230 electron microscope with a LaB_6 filament, operating at an accelerating voltage of 100 kV.

The visible light transmittance of the nanocomposite film was measured by a UV-Vis spectrometer (Perkin-Elmer Lambda 35). The refractive index of the nanocomposite films was determined by using a Metricon Prism Coupler 2010/M with a helium neon laser of 633 nm (Melles Griot, 05-LHP-073-515).

The Young's modulus and Vickers hardness of the nanocomposite were performed on the disk samples using a UMIS II (Ultra-micro indentation system) pyramid-shaped indenter (CSIRO) at a maximum force load of 5 mN.

The coefficient of thermal expansion (CTE) and glass transition temperature of the nanocomposites were measured in nitrogen from 30 to 200 °C at a heating rate of 5 °C min^{-1} by using a thermal mechanical analyzer (TA instruments TMA-2940). The decomposition temperature (Td) of the nanocomposites was measured in air from room temperature to 600 °C with a heating rate of 10 °C min^{-1} by a thermal gravimetric analyzer (TA instruments TGA-2950).

The water absorption of the nanocomposite was determined by weight difference before and after water absorption. The disk samples were weighed first after drying at 100 °C for 24 h and then cooling down to room temperature in a desiccator. The dried samples were refluxed in de-ionized water at 100 °C for 24 h. After the reflux, the disk samples were weighed after cooling down to room temperature and wiping off the surface water. Then, the water absorption of each nanocomposite was calculated from the weight change.

The water vapor permeability of nanocomposite films was determined by using permeability cups (S-1003, Sheen Instruments) in a temperature and humidity controlled environmental chamber (Terchy HRM-80FA, Taichy Tech. Co., Taiwan). The film thickness is about 100 μm and the test area is 10 cm^2. The test method followed the ASTM E 96 method. We have included the film thickness in the calculation to obtain specific permeability.

The water contact angle of the nanocomposite film was determined using a contact angle analyzer (FTA125, Ten Angstroms, Inc.). Five contact angle measurements were performed for each sample, and then the average and standard deviation of the data were calculated. The surface morphology of NES60 and NPS60 films coated with platinum was studied by a JOEL JSM-6700F field emission scanning electron microscope at an accelerating voltage of 10 kV.

The adhesive property of the nanocomposite film on a glass substrate was determined by the crosshatch test according to the ASTM D3559 method.

All the data obtained from characterizations are tabulated in a Table in the supplementary information.

Results and discussion

Synthesis and characterization of photosensitive fluoroimide acrylate oligomer (PSFIA)

Scheme 1 illustrates the synthetic scheme for the preparation of photosensitive fluoroimide acrylate oligomer (PSFIA). A 2 times excess equivalent amount of dianhydride 6FDA was used to react with diamine 6FpDA to obtain dianhydride terminated fluoroimide (FIDA). The FIDA was reacted further with 2 moles of hydroxyl ethyl methacrylate (HEMA) to obtain PSFIA. The FTIR spectrum of FIDA shows characteristic absorption bands of 718, 1372, 1729, 1787 cm^{-1} for the imide group and 1858 cm^{-1} for the cyclic anhydride group (supplementary information). The

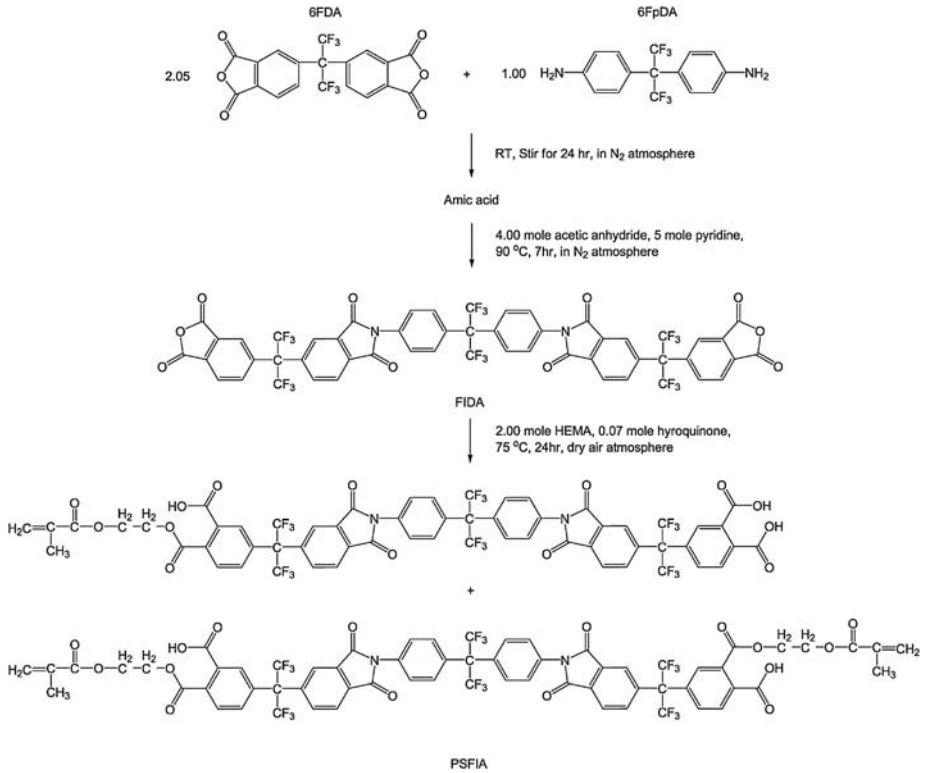

Scheme 1 Synthetic scheme for PSFIA oligomer.

FTIR spectrum of PSFIA exhibits characteristic absorption bands of the acrylate ester of 1608 cm^{-1} (C═C) and 1720 cm^{-1} (C═O), and the carboxylic acid of 3500 cm^{-1} (COOH). The acid functionality is designed into the fluoroimide resin system to increase its affinity toward SiO_2 nanoparticles and glass substrate.

The ^1H NMR of FIDA and PSFIA are used to determine the chemical structure and the molecular weight of FIDA and PSFIA (supplementary information). We designate protons of monomer A (6FpDA) as a and b; protons of monomer B (6FDA) as c, d and e; protons of the acrylate functional group of monomer C (HEMA) as f, g, h, i and j. By integration of each type of proton area and taking the ratio of specific proton area to the total proton area before and after the reaction, we have determined that the structure of FIDA is BAB and the structure of PSFIA is a mixture of C-BAB-C (17 mole %) and C-BAB (83 mole %).

The resin part of the nanocomposite contains 30 wt% PSFIA and 70 wt% of neopentyl glycol diacrylate (NPGDA). The NPGDA is an acrylate monomer that dissolves PSFIA powder and adjusts the flow behavior of the resin. Then different amounts of 3-(trimethoxysilyl) propyl methacrylate modified SiO_2 nanoparticles are dispersed into the resin to obtain resin systems containing 10, 20, 30, 40, 50 and 60 wt% SiO_2, respectively. In order to gain insight into the chemical structure effect of fluoroimide acrylate on the performance of the nanocomposite, we have used ethoxylated bisphenol A diacrylate (EOBDA) as a control. The resin system made from PSFIA is called the NPS series and the resin system made from EOBDA is called the NES series. The chemical composition and the acrylate functionality of the resin systems are summarized in Table 1.

Physical and chemical properties of the nanocomposite

The physical and chemical properties of the nanocomposite are greatly influenced by the crosslinking density of the nanocomposite. The crosslinking density will be higher if the acrylate functionality is higher in the resin system. The theoretical acrylate functionality can be calculated from the resin composition. The acrylate functionality is decreased with increasing the amount of MPS modified nanoparticle based on the total weight of the organic matrix and nanoparticle (Table 1 column 7). However, the acrylate functionality is increased with increasing the amount of MPS modified nanoparticle based on the weight of the organic matrix (Table 1 column 8), because the amount of acrylate coupling agent MPS is increased with increasing the amount of nanoparticle.

The adhesive properties of the nanocomposite are evaluated by the crosshatch adhesion test on a glass substrate. It is interesting to note that the NPS series fluoroimide acrylate nanocomposite exhibits much better adhesion properties than the NES series nanocomposite. For example, at 40 wt% SiO_2 concentration, the crosshatch adhesion is <35% (0B), >85% (4B) for NES40 and NPS40, respectively. The unusually good adhesive performance of the NPS series is due to the acidic functionality of PSFIA which could form strong chemical bonding with glass. As compared with the NES series, the lower acrylate functionality of the NPS series also contributes to the good adhesion because the shrinkage is less after the polymerization.

The UV-Vis spectra of nanocomposite films are shown in Fig. 1 (a) and 1 (b). The samples of the NPS and NES series exhibit no drastic transmittance changes with an increase of SiO_2 content in the region of 400–800 nm. The transmittance of the

NPS series samples (>89%) is not as good as the NES series (>95%) in this wavelength range. The transmittance decreases for both series below 400 nm which is due to the scattering of the nanoparticles.[27] However, the extent of decrease is more in the NPS series than that in the NES series. The NPS10 and NPS20 samples containing the least amount of SiO_2 exhibit the lowest transmittance around 400 nm but the transmittance of NPS series nanocomposite is improved with increasing SiO_2 content. The scattering from nanoparticles alone cannot explain the large decrease in transmittance of the NPS series. As we compare the TEM morphology differences between NES series (Fig. 2a, 2b and 2c), and NPS series (Fig. 2d, 2e and 2f), the dispersion of SiO_2 nanoparticles of the NES series is obviously better than that of NPS series. Nanosize aggregations (Fig. 2d) are formed in the NPS series that are due to the interfacial interaction between the nanoparticles and fluoroimide acrylate resin. The aggregations (~50–100 nm, Fig. 2d) are larger than the nanoparticle individually isolated by resin (~20 nm, Fig. 2a) which results in large scattering and low transmittance. The transmittance of the NPS series is increased by increasing of the amount of SiO_2 nanoparticle (Fig. 1b) because the aggregation decreases with a smaller amount of fluoroimide acrylate resin (Fig. 2e and 2f). The morphology of the nanocomposite is controlled by the interfacial interactions between nanoparticles and resin. The hydrophobic characteristic of the fluoroimide acrylate resin shows less compatibility with SiO_2 nanoparticle as compared with ethoxylated bisphenol A acrylate resin (EOBDA). The phase separation between the fluoroimide acrylate oligomer and the SiO_2 nanoparticle occurs and aggregates are formed. The detailed comparison of hydrophobicity between the NES series and the NPS series will be discussed later.

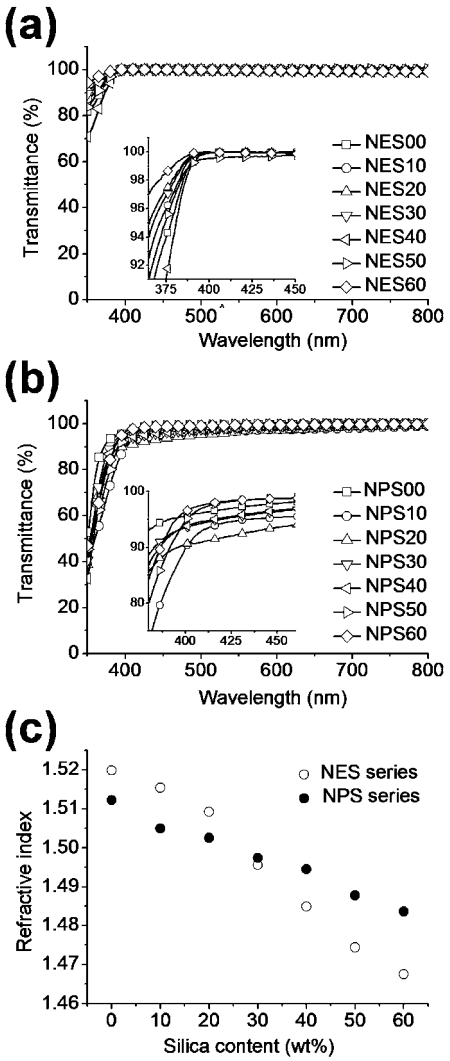

Fig. 1 Transmittance of nanocomposites: (a) NES series and (b) NPS series, (c) refractive indexes of NES series and NPS series nanocomposites.

Fig. 1c compares the refractive index differences between NES and NPS series nanocomposites at different SiO_2 content. The refractive index of NPS neat polymer (NPS00) is intrinsically lower than that of NES neat polymer (NES00) due to the presence of fluorine in the polymer. As expected, the refractive index of both nanocomposites decreases with increasing content of low refractive index SiO_2. The extent of decrease of refractive index of the NPS series follows the addition rule of blending systems. However, the extent of decrease of the refractive index of the NES series does not follow the addition rule and its curve shows two slopes. It is interesting to observe that the refractive index of the NES60 sample (containing 60 wt% SiO_2) is almost equal to the refractive index of fused SiO_2[28] (1.4675 *vs.* 1.4570). The result indicates that the compatibility between the NES polymer and SiO_2 nanoparticles is much better than the compatibility between the NPS polymer and SiO_2 nanoparticles which is consistent with the TEM results (Fig. 2). It has been reported that the refractive index of well dispersed nanocomposite systems does not follow the addition rule.[4] When the amount of nanoparticles is greater than the percolation threshold of the network, the properties of nanoparticles dominate.[29]

As expected, the micro-hardness and Young's modulus of both NES and NPS series nanocomposites are increased with increasing the content of SiO_2 (Fig. 3). The nonlinear relationship is present in both systems due to the formation of a percolation network at a higher content of SiO_2 as shown in the TEM photos (Fig. 2b, 2c, 2e and 2f). The NES neat polymer has higher acrylate functionality (*e.g.* higher crosslinking density) than the NPS neat polymer, thus the former exhibits a higher microhardness. However, the Young's modulus of NPS neat polymer is higher than that of NES neat polymer. The fluoroimide moiety of polyfluoroimide acrylate is expected to provide stronger mechanical toughness as compared with pure polyacrylate obtained from ethoxylated bisphenol A diacrylate.

Fig. 4 shows the NES neat polymer exhibits a higher Td than the NPS neat polymer due to the former has higher acrylate functionality resulting in higher crosslinking density (see Table 1). The extent of increase of the Td of the nancomposite with increasing content of SiO_2 is higher for the NPS series as compared with the NES series because the increasing rate of acrylate functionality is higher in the NPS series (see Table 1). From the chemical structure effect point of view, the fluoroimide acrylate itself should be more thermally stable. However, the oligomer PSFIA of the NPS series has a higher molecular weight and mono acrylate functionality that results in a lower acrylate functionality of the NPS neat polymer as compared with the NES neat polymer.

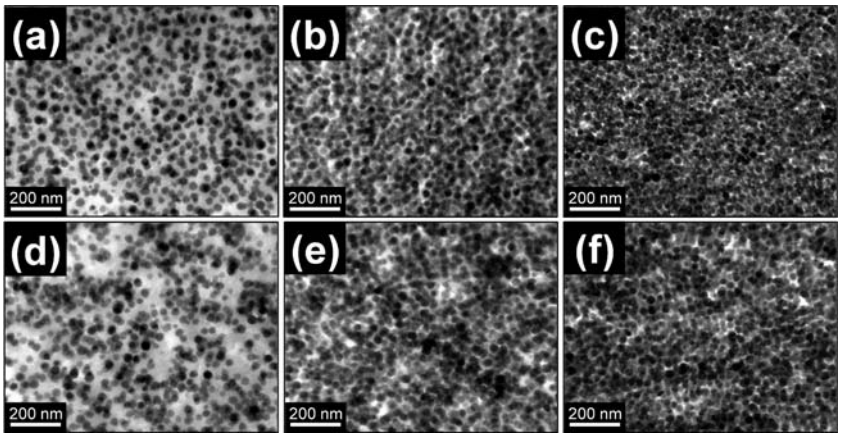

Fig. 2 TEM images of nanocomposites: (a) NES20, (b) NES40, (c) NES60, (d) NPS20, (e) NPS40 and (f) NPS60.

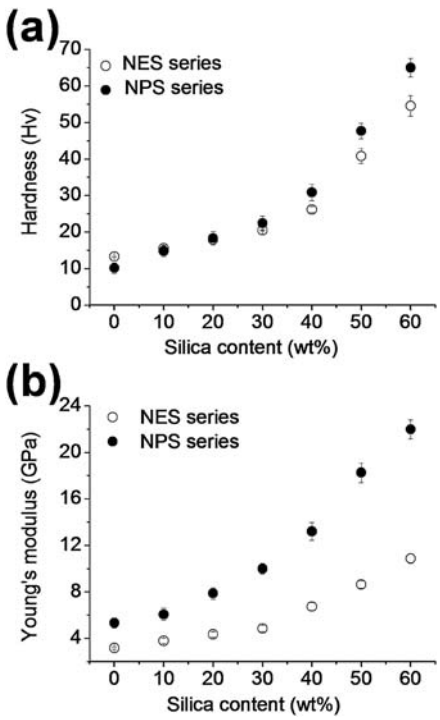

Fig. 3 Comparison of micro-hardness (a) and Young's modulus (b) between the NES and NPS series nanocomposites.

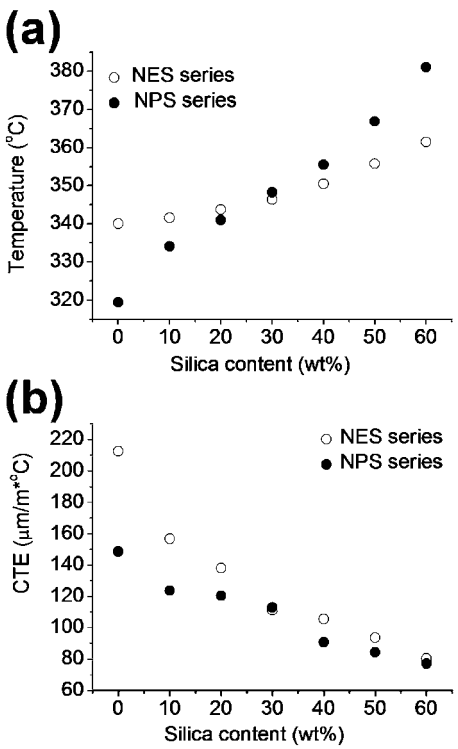

Fig. 4 Comparison of decomposition temperature (a) and coefficient of thermal expansion (b) between the NES series and the NPS series nanocomposites.

We have used contact angle measurement to evaluate the hydrophobicity of the neat polymer and nanocomposite (see supplementary information). As expected, the NPS series shows a larger contact angle than that of the NES series (Fig. 5a). The pure polyacrylate made from EOBDA shows a contact angle of about 71° due to its hydrophilic poly(ethylene oxide) structure. The T-PFSIA exhibits a high contact angle of about 100° from the hydrophobicity of the fluoroimide moiety that overrides the hydrophilicity of polar acrylate and carboxylic acid moieties. By adding 70 wt% of NPGDA monomer into the PSFIA, the contact angle of PSFIA decreases to about 82° because the NPGDA is more hydrophilic than the PSFIA. The contact angle of the nanocomposite increases with increasing content of SiO_2 nanoparticles, which results from the nano roughness created by the nanoparticles (Fig. 5d). It is interesting to observe that the extent of contact angle increase is higher for the NPS series than the NES series. The difference may be from the formation of SiO_2 nanoparticle aggregates in the NPS series which has been observed in the TEM image of NPS 20 (Fig. 2d). Fig. 5 clearly indicates that NPS60 has a rougher surface than NES60. This results in a higher contact angle of NPS60 as compared with NES60. The nanosize aggregates increase surface roughness thus enhancing the hydrophobicity of nanocomposite NPS60. The NPS60 still exhibits good transparency (96.44% at 400 nm) because its surface roughness and aggregate size are smaller than 100 nm with minor light scattering. Therefore, high

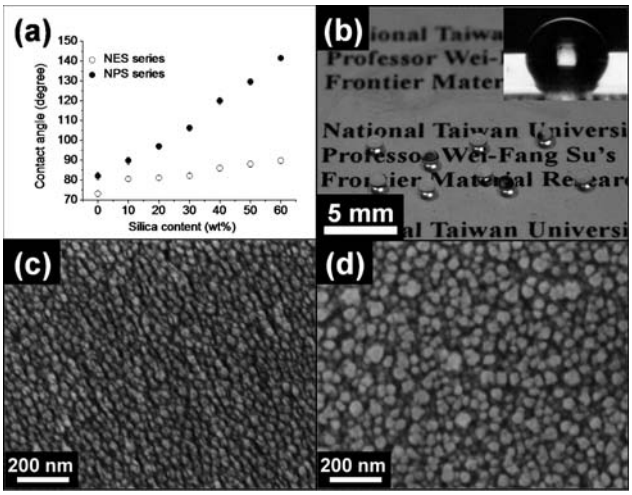

Fig. 5 (a) Comparison of contact angles between NES and NPS series, (b) water droplets on the surface of highly transparent NPS60 coated on glass and the inset shows the contact angle of the film is 142°. SEM images of nanocomposites (c) NES60 and (d) NPS60.

hydrophobicity of the NPS series nanocomposites can be achieved by increasing the content of SiO_2 without decreasing its transparency. Fig. 5b demonstrates that a large area of highly transparent and hydrophobic coating can be easily obtained by UV-curing of NPS60. There is no solvent and high temperature calcination involved in the process.

The material used for device encapsulation has to have the properties of low water absorption and low water vapor permeation. These two properties have been studied for the nanocomposites of the NPS series and NES series. The results are shown in Fig. 6. The NPS series shows much lower water absorption and water vapor permeability than those of the NES series due to the presence of the more hydrophobic fluoroimide group. When the SiO_2 content of the nanocomposite increases, the barrier properties of both the NES series and NPS series nanocomposites are enhanced. The results are expected because SiO_2 is denser than the organic matrix and less water permeation is possible. However, the decrease of water absorption and water vapor permeability of the NES series is more obvious than that of the NPS series. Both inorganic and organic components of the nanocomposites play a role in water absorption and water permeation behaviors. Apparently, the enhancement of barrier properties contributed by spherical SiO_2 nanoparticle is not obvious for the nanocomposite made from polyfluoroimide acrylate which itself has good barrier properties.

Conclusions

We have successfully synthesized a hydrophobic photosensitive fluoroimide acrylate oligomer containing carboxylic acid functionality that can be easily blended with acrylate monomer, acrylate modified SiO_2 nanoparticle and photoinitiator to make an environmentally friendly and energy conserving solventless photocurable resin system for fabricating nanocomposites. The nanocomposite exhibits excellent performance including high transparency, good adhesive strength, good thermal stability, high mechanical durability and low moisture permeation. As

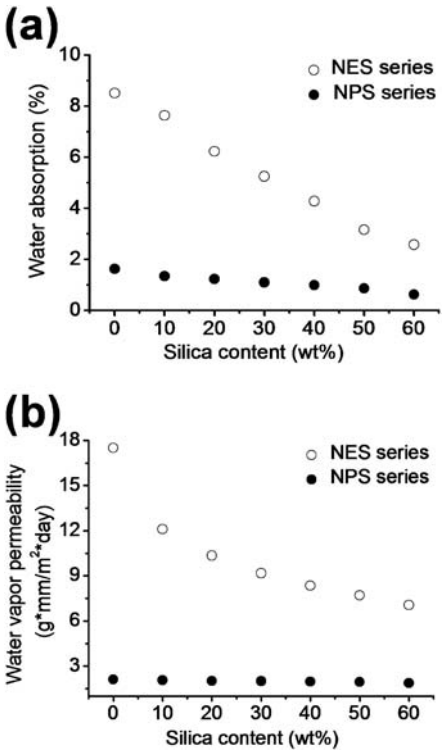

Fig. 6 Comparison of water absorption (a) and water vapor permeability (b) between the NES series and NPS series nanocomposites.

compared with conventional non-fluoro oligomers, the fluoro oligomer plays a major role in the enhancement of the physical and chemical properties of the nanocomposite in addition to the contribution from the nanoparticles. This new novel nanocomposite will be useful for applications in optics, waveguides and device encapsulation.

Acknowledgements

We are grateful for financial support from the National Science Council of Taiwan (95-3114-P-002-003-MY3) and the U.S. Air Force (AOARD-07-4014).

Reference

1 A. C. Balazs, T. Emrick and T. P. Russell, *Science*, 2006, **314**, 1107–1110.
2 R. A. Vaia and E. P. Giannelis, *MRS Bull.*, 2001, **26**, 394–401.
3 K. I. Winey and R. A. Vaia, *MRS Bull.*, 2007, **32**, 314–319.
4 W. F. Su, J. F. Lee, M. Y. Chen and R. M. Ho, *J. Mater. Res.*, 2004, **19**, 2343–2348.
5 N. Nakayama and T. Hayashi, *Composites, Part A*, 2007, **38**, 1996–2004.
6 J. U. Park, W. S. Kim and B. S. Bae, *J. Mater. Chem.*, 2003, **13**, 738–741.
7 C. Y. Lee, Y. T. Haung, W. F. Su and C. F. Lin, *Appl. Phys. Lett.*, 2006, **89**, 231116.
8 T. W. Zeng, Y. Y. Lin, H. H. Lo, C. W. Chen, C. H. Chen, S. C. Liou, H. Y. Huang and W. F. Su, *Nanotechnology*, 2006, **17**, 5387–5392.
9 W. U. Huynh, J. J. Dittmer and A. P. Alivisatos, *Science*, 2002, **295**, 2425–2427.
10 L. H. Lin, H. J. Liu and N. K. Yu, *J. Appl. Polym. Sci.*, 2007, **106**, 260–266.
11 M. Pluta, J. K. Jeszka and G. Boiteux, *Eur. Polym. J.*, 2007, **43**, 2819–2835.
12 M. H. Chen, C. R. Chen, S. H. Hsu, S. P. Sun and W. F. Su, *Dent. Mater.*, 2006, **22**, 138–145.

13 K. K. Baikerikar and A. B. Scranton, *Polymer*, 2001, **42**, 431–441.
14 J. N. Tey, A. M. Soutar, S. G. Mhaisalkar, H. Yu and K. M. Hew, *Thin Solid Films*, 2006, **504**, 384–390.
15 A. Nakajima, A. Fujishima, K. Hashimoto and T. Watanabe, *Adv. Mater.*, 1999, **11**, 1365–1368.
16 K. Tadanaga, J. Morinaga, A. Matsuda and T. Minami, *Chem. Mater.*, 2000, **12**, 590–592.
17 K. Tadanaga, J. Morinaga and T. Minami, *J. Sol-Gel Sci. Technol.*, 2000, **19**, 211–214.
18 A. Nakajima, K. Hashimoto, T. Watanabe, K. Takai, G. Yamauchi and A. Fujishima, *Langmuir*, 2000, **16**, 7044–7047.
19 J. Bravo, L. Zhai, Z. Z. Wu, R. E. Cohen and M. F. Rubner, *Langmuir*, 2007, **23**, 7293–7298.
20 R. Taurino, E. Fabbri, M. Messori, F. Pilati, D. Pospiech and A. Synytska, *J. Colloid Interface Sci.*, 2008, **325**, 149–156.
21 Q. F. Xu, J. N. Wang, I. H. Smith and K. D. Sanderson, *J. Mater. Chem.*, 2009, **19**, 655–660.
22 M. Manca, A. Cannavale, L. De Marco, A. S. Arico, R. Cingolani and G. Gigli, *Langmuir*, 2009, **25**, 6357–6362.
23 Y. Li, F. Liu and J. Q. Sun, *Chem. Commun.*, 2009, 2730–2732.
24 A. Steele, I. Bayer and E. Loth, *Nano Lett.*, 2009, **9**, 501–505.
25 M. Sangermano, R. Bongiovanni, M. Longhin, G. Rizza, C. M. Kausch, Y. Kim and R. R. Thomas, *Macromol. Mater. Eng.*, 2009, **294**, 525–531.
26 H. Zou, S. S. Wu and J. Shen, *Chem. Rev.*, 2008, **108**, 3893–3957.
27 I. S. Liu, Y. F. Chen and W. F. Su, *J. Photochem. Photobiol., A*, 2008, **199**, 291–296.
28 I. H. Malitson, *J. Opt. Soc. Am.*, 1965, **55**, 1205–1208.
29 C. C. Lin, K. H. Chang, K. C. Lin and W. F. Su, *Compos. Sci. Technol.*, 2009, **69**, 1180–1186.